Waveform Selection for FMCW and PMCW 4D-Imaging Automotive Radar Sensors

Nazila Karimian Sichani[*1], Moein Ahmadi[2], Ehsan Raei[2],
Mohammad Alaee-Kerahroodi[2], Bhavani Shankar M. R.[2], Esfandiar Mehrshahi[1], Seyyed Ali Ghorashi[3,1]

[1]*Department of Telecommunications, Faculty of Electrical Engineering, Shahid Beheshti University, Tehran 1983963113, Iran.*
[2]*Interdisciplinary Centre for Security, Reliability and Trust (SnT), University of Luxembourg, Luxembourg.*
[3]*Department of Computer Science and Digital Technologies, School of Architecture, Computing and Engineering,*
University of East London, E16 2RD, London, UK.

Abstract—The emerging 4D-imaging automotive MIMO radar sensors necessitate the selection of appropriate transmit waveforms, which should be separable on the receive side in addition to having low auto-correlation sidelobes. TDM, FDM, DDM, and inter-chirp CDM approaches have traditionally been proposed for FMCW radar sensors to ensure the orthogonality of the transmit signals. However, as the number of transmit antennas increases, each of the aforementioned approaches suffers from some drawbacks, which are described in this paper. PMCW radars, on the other hand, can be considered to be more costly to implement, have been proposed to provide better performance and allow for the use of waveform optimization techniques. In this context, we use a block gradient descent approach to designing a waveform set that is optimized based on weighted integrated sidelobe level in this paper, and we show that the proposed waveform outperforms conventional MIMO-FMCW approaches by performing comparative simulations.

Index Terms—4D-Imaging, Automotive Radar, FMCW, PMCW, CDM-MIMO, WISL.

I. Introduction

To meet the requirement of high-resolution sensing capabilities in the range–Doppler–azimuth–elevation domains, Advanced Driver Assistant Systems (ADAS) require 4D-Imaging radars in emerging automotive applications. With this regard, a large antenna array aperture is needed that can be obtained using sparse configuration based on Multiple-Input Multiple-Output (MIMO) concept. MIMO radars can enlarge the aperture size virtually, by reducing the number of physical transmit and receive antenna elements that construct the desired aperture size, in both elevation and azimuth. However, increasing number of transmit antennas enlarges the complexity of the transmit waveforms, which is a subject of discussion in Frequency-Modulated Continuous-Wave (FMCW) and Phase-Modulated Continuous-Wave (PMCW) radar systems.

As compared to FMCW radars, PMCW radars show good properties in terms of interference mitigation [1]. However, due to the high instantaneous bandwidth, digitally modulated waveforms in PMCW radars raise high sampling rate in Analog to Digital Converter (ADC)s, which increase the cost of implementation [2]. On the other hand, using orthogonal

codes allow us to transmit orthogonal waveforms from all transmitters in PMCW MIMO radars simultaneously, in fast-time domain. On the contrary, generating orthogonality is a difficult task to achieve in FMCW radars and can only be implemented over time, frequency, Doppler, or in slow-time.

In this paper, we provide a comprehensive summary of different multiplexing techniques to transmit orthogonal waveforms and discuss about their advantages and disadvantages. We also provide a unified signal model through which different modulation schemes can be implemented. For the case of PMCW radars, we propose an optimization framework based on Gradient Descent (GD) to design set of sequences which exhibit good orthogonality and low sidelobe levels in their correlation functions. The numerical results validate the proposed algorithm's performance for a 4D imaging radar example[1].

II. Transmit and Receive Signal Models

We consider a colocated MIMO radar sensor, with M transmit and N receive antenna elements. Let

$$\mathbf{u}_{m,q}(t) = \sum_{k=1}^{K} w_{m,q} e^{j\phi_{m,k}} rect\left(\frac{t-kT_c-\frac{T_c}{2}}{T_c} - \frac{T_p}{2}\right) \quad (1)$$

be the qth transmitted radar pulse[2] from m^{th} transmit antenna with K subpulses of duration T_c (chip-time), resulting in a coded pulse of T_p duration. With arbitrary selection of $\phi_{m,k}$, (1) indicates the transmitted signal for PMCW MIMO radars, but by setting $\phi_{m,k} = \beta\pi(kT_c)^2$, the same equations shows FMCW waveform where β is the chirp rate [3]. Additionally, $w_{m,q}$ generates different orthogonality weights for a MIMO transmission, as specified in TABLE I for Time-Division Multiplexing (TDM), Doppler-Division Multiplexing (DDM), and Binary Phase Modulation (BPM)[3] cases. For fast-time Code-Division Multiplexing (CDM), we can choose $w_{m,q} = 1$. Assuming that a total of Q pulses are transmitted in every Coherent Processing Interval (CPI), the emitted signal from each

---

[1]**Notation**: We use boldface upper case $\mathbf{X}$ for matrices and boldface lower case $\mathbf{x}$ for vectors. The sets of complex number, real number, Hadamard product, Frobenius norm, phase of vector and matrix, hermitian operation, correlation, gradient, round and rectangular functions are denoted by, $\mathbb{C}^N$, $\mathbb{R}^N$, $\Im(.)$, $\odot$, $||.||_F$, $\angle.$, $(.)^H$, $\circledast$, ∇, $\lfloor.\rfloor$ and $rect(.)$ respectively.

[2]We split the time index into fast-time (p) and slow-time (q) (i. e., $t = p/f_s + qT_p$) with f_s as the sampling rate.

[3]Called slow-time CDM, when the alphabet size is not limited to binary.

TABLE I: The weight parameter for generating TDM, DDM, and BPM-MIMO signals. Here, δ is Dirac delta function, had is Hadamard matrix and mod performs a remainder operation.

Technique	$w_{m,q}$
TDM	$\delta[m - mod(q-1, M) - 1]$
DDM	$e^{-j2\pi mq/M}$
BPM (Hadamard)	$had[m, mod(q-1, M) + 1]$

transmitting antenna is, $\mathbf{s}_m(t) = \sum_{q=1}^{Q} \mathbf{u}_{m,q}(t - qT)e^{j2\pi f_c t}$, where f_c is the carrier frequency, and T is Pulse Repetition Interval (PRI) which depends on the duty cycle of the transmitting that waveform may or may not be equal to T_p. The reflected signal from I moving targets, $i = 1, 2, \ldots, I$, is,

$$\mathbf{y}_n(t) = \sum_{i=1}^{I} \sigma_i \sum_{m=1}^{M} \mathbf{s}_m(t - \tau_i), \qquad (2)$$

where σ_i is the reflection coefficient from i^{th} target, and $\tau_i = \tau_{0,i} + \tau_{d,i} + \tau_{s,i}$. Here, $\tau_{0,i} = \frac{2R_i}{c}$, where R_i is the distance and c is the light speed, is the round-trip time related to the distance of ith target with radar; $\tau_{d,i} = \frac{2\nu_i t}{c}$ is due to the speed of the ith target and includes Doppler information; and $\tau_{s,i} = \sin\theta_i(md_t + nd_r)^4$ is caused by the phase differences between the mth transmit antenna element and n^{th} receive antenna element (determines so-called transmit and receive array steering vectors) for a target at angle θ_i, with d_t and d_r as the transmitter and receiver inter-element spacing, respectively. The received signal is then processed at each receiver for target parameter estimation.

A. Signal Processing in FMCW radars

In automotive radars, FMCW is typically used as the standard modulation scheme, since it can be compressed with a very low-cost and efficient technique known-as *de-chirping* operation (stretch processing) [1], [4]. The primary benefit of de-chirping is that the received signal can be sampled at much lower rates in comparison to its bandwidth. Not surprisingly, this advantage has been motivating many automotive manufactures to build their radar system based on FMCW technology.

Using the de-chirping technique, the received signal is conjugately mixed with a source chirp to produce Intermediate Frequency (IF) signal. With some manipulations on (2), the IF signal as a function of fast-time and slow-time at the nth receive antenna element can be expressed as [5]:

$$\mathbf{Z}_{n,p,q} = \sum_{i=1}^{I} \sum_{m=1}^{M} \sigma_i w_{m,q} e^{-j2\pi(\beta\tau_{0,i} + f_{d,i})p/f_s}$$
$$e^{-j2\pi f_{d,i}qT} e^{-j\frac{2\pi}{\lambda}(md_t + nd_r)\sin\theta_i} \qquad (3)$$

where $\lambda = c/f_c$ is the wavelength, $f_{d,i} = 2\nu_i/\lambda$ is the ith target Doppler shift. The first, second and third exponential terms in (3) are used for range, Doppler and angle estimation of the target, respectively. In the case of MIMO transmission, a decoding process is required to separate the transmitted signals in the receive depending on how $w_{m,q}$ is weighted.

---

[4] In general, $\tau_{s,i}$ is a function of antenna positions and also azimuth (θ_i)-elevation (ϕ_i) angles of the target. For simplicity, we consider a Uniform Linear Array (ULA) setting in the signal model, which cause $\tau_{s,i}$ be only depended on θ_i and the array parameters m, n, d_t and d_r.

B. Signal Processing in PMCW radars

The received signal in PMCW radars is down-converted to baseband (i.e., $\tilde{\mathbf{y}}_n(t) = \mathbf{y}_n(t)e^{-j2\pi f_c t}$), then passed through the matched-filter, or pulse compression filter, corresponding to each transmitting waveform at each single receiver. At the output of the matched-filter with the mth transmit waveform, for the nth receive element, we have:

$$\mathbf{Z}_{m,n,q}(t) = \int_{-\infty}^{\infty} \tilde{\mathbf{y}}_n(\tilde{\tau})\mathbf{u}_{m,q}^*(\tilde{\tau} - t)d\tilde{\tau}, \qquad (4)$$

substituting the received signal and after sampling, we obtain,
$$\mathbf{Z}_{m,n,q,p} = \mathbf{Z}_{m,n,q}(p/f_s) =$$
$$\sum_{i=1}^{I} \sum_{l=1}^{M} \sum_{q=1}^{Q} \sigma_i r_{m,l}(p - \lfloor f_s\tau_{0,i}\rfloor)$$
$$e^{-j2\pi f_{d,i}qT} e^{-j\frac{2\pi}{\lambda}(md_t + nd_r)\sin\theta_i}$$

where $r_{m,l}(.)$ is the cross-correlation function between m^{th} and l^{th} transmit waveforms and $p = 1, \ldots, \lfloor 2R_{max}f_s/c \rfloor$ and R_{max} is the maximum range of interest.

III. WAVEFORM SELECTION FOR FMCW AND PMCW MIMO RADAR SENSORS

The choice of waveform in the automotive MIMO radars is critical because it influences both radar performance and implementation complexity. MIMO radar waveforms should possess low auto-correlation sidelobes, and be chosen from an orthogonal set to be separated in the receive side.

A. Orthogonal Set Generation for FMCW MIMO Radars

Different modulation schemes, such as TDM, Frequency Division Multiplexing (FDM), DDM, and (slow-time) CDM, have been presented in the literature to generate a set of orthogonal waveforms based on FMCW.

The TDM-based multiplexing technique is the most widely employed in the conventional automotive radar due to its low hardware complexity. This modulation allocates a different time slot to each transmitter in order to produce orthogonal transmitting waveforms (in time domain) and ensures the ideal orthogonality [6]. With this regard, each transmit antenna has an exclusive access to the radar channel within a relatively short time period. On the other hand, all receive antennas operate simultaneously [7]–[10].

Although low cost and easily implemented, TDM requires longer measurement time, strict synchronization between transmit and receive side, and additional effort for estimation of moving target velocity. Furthermore, TDM-MIMO radars suffer from the transmit energy loss, leading to a reduced Signal to Noise Ratio (SNR). As a result, it reduces the target detection range and degrades the parameter estimation performance with increasing the number of transmit elements [5]. One major drawback of TDM-MIMO technique is the ambiguity in maximum Doppler velocity estimation, which is proportional to the inverse of the number of transmit antenna elements. Thus, in 4D-imaging automotive radars, due to the requirement of large number of transmit antenna elements, the maximum unambiguous velocity in TDM structure will be significantly reduced, compared to the fewer number of transmit antennas scenario. This degradation in velocity estimation

will also corrupts the Direction Of Arrival (DOA) estimation, which cause a coupling between target angle and velocity [7]. This coupling leads to an additional phase component in the array steering vector of the virtual transmit antenna elements. In order to tackle the above-mentioned limitations of the TDM-MIMO, some alternatives to the TDM-based FMCW radar were proposed in the literature.

Unlike the TDM technique, FDM can produce transmitting signals that are concurrently sent but distinct from one another in the frequency domain. To this end, the transmitted signals (e. g., FMCW) are modulated by different carrier frequencies [11]. In the conventional FDM, the frequency shifts are equal to the bandwidth of transmitted signals from each antennas. In this case, the problem of Doppler ambiguity limit which was discussed in TDM case is being solved. Furthermore, FDM achieves higher SNR compared to TDM. On the other side, due to the need for large bandwidth, it leads to a waste of frequency resources and bandwidth loss, and has a high implementation cost. Also, a range-angle coupling problem will occur. A randomization of the frequency shift among transmit antennas reduces this range-angle coupling. However, a large number of transmit antennas is needed for this purpose, which is feasible for 4D-imaging radars [12]. But, due to the large occupied bandwidth in 4D-imaging automotive radars, using conventional FDM is not efficient. On the other side, there are other types of FDM waveforms, like DDM, which only depends on some frequency offsets.

DDM-MIMO is a low-complex multiplexing technique that, like in FDM, shifts each transmitting signal spectrum, using a sequence of phase shifters. The difference is that only a slight Doppler frequency step size is needed such that it can enable signal separation in Doppler domain [13]. DDM has been widely implemented in automotive radars, due to the high performance-to-cost ratio [14], [15]. Two requirements ought to be considered for the frequency step size in DDM structure. First, The frequency shifts in DDM should be greater than two times of the fastest target Doppler shift to ensure separation in Doppler domain. Second, to guarantee the orthogonality, the frequency step size has to be equal or greater than the inverse of pulse duration time [6]. DDM Improves the problem of limited frequency spectrum resources in FDM (due to the small frequency offset) and long measurement time in TDM (due to simultaneous transmitting). Nonetheless, orthogonal waveforms in Doppler domain suffer from the reduction in the maximum unambiguous Doppler and the maximum detectable velocity, since the received signals are aliased in Doppler domain. As a result, DDM-MIMO is mostly fits to Short Range Radar (SRR) applications. To solve the problem of Doppler ambiguity in DDM, different approaches, like TB-DDM [5] and dithered-DDM [16], were proposed in the literature.

CDM among chirps can be applied in both fast-time and slow-time domains. In the slow-time chirp coding, each separate chirp is multiplied by a code symbol (inter-chirp CDM), and it is in fact equivalent to the conventional DDM approach, with similar advantages and disadvantages. There is also a variation of CDM which has been applied in fast-time and

is called intra-chirp coding [17]. Inter-chirp coding provides significantly lower range sidelobs in the ambiguity function compared to the intra-chirp coding. As a result, in automotive radar applications, inter-chirp coding has been widely used [17]. In this context, there exists special binary code with near perfect orthogonality for inter-chirp coding, which is the Hadamard code [5]. Since inter-chirp CDM-MIMO utilizes various phase-codes for transmitted signals, in the same frequency and time, it necessitates a decoding process at the receive side to separate the transmitting signals.

B. Orthogonal Set Design for PMCW MIMO Radars

Another orthogonalization scheme that is used recently in automotive radars, is based on CDM, which in principle is suitable for PMCW radars [18]–[21]. CDM-MIMO based on intra-pulse coding, which is a systematic approach in many different radar applications, and utilizes set of sequences with good auto- and cross-correlation properties [1], [22]–[25]. This scheme is a suitable solution for fast 4D-Imaging automotive applications, since it supports simultaneous transmitting in both time and frequency. The advantage of using CDM is that it overcomes the above-mentioned drawbacks for TDM, FDM, or BPM, and achieves higher SNR and higher range resolution in comparison with TDM and FDM, respectively. However, it suffers from difficult hardware implementation. Also, due to the cross-correlation among the codes, it is difficult to achieve perfect orthogonality, unlike TDM and FDM. Thus, the properties of the code set such as auto-correlation and cross-correlation highly influence the performance of the CDM. The noise floor and range ambiguity limit the radar performance in the case of CDM. To adequately distinguish between the multiple targets, the codes should have very low cross-correlation values. The multiple-source interference levels are controlled by the cross-correlation level as well as the relative power level of the received signals. Hence, finding a code set that satisfies the radar system requirement is challenging, but has been well studied and addressed in several recent papers [25].

IV. WAVEFORM OPTIMIZATION

There are several metrics available for designing a set of sequences with good orthogonality in PMCW radars [26], one of which is Weighted Integrated Side-lobe Level (WISL) [25]. The aim here is to reduce the auto- and cross-correlation sidelobes of a sequence set as much as possible in a Regions Of Interest (ROI), which can be calculated in principle based on the radar system's maximum detection range. This methodology is useful when the pulse time T_p in (1) is much greater than the delay of $\tau_{0,i}$, $i = 1, 2, \ldots, I$, as in PMCW automotive radar applications.

Let us assume that $\mathbf{X} \in \mathbb{C}^{M \times K}$ is the set of transmitted sequences in baseband with M transmit antennas and K samples for each transmitter, and $x_{m,k} = e^{j\phi_{m,k}}$ is the kth sample of mth antenna. We aim to solve the following optimization problem:

$$\begin{cases} \min_{\mathbf{X}} & f(\mathbf{X}) \triangleq \sum_{m=1}^{M}\sum_{l=1}^{M}\sum_{k=-K+1}^{K-1}|\alpha_{m,l}(k)r_{m,l}(k)|^2 \\ & \quad - \sum_{m=1}^{M}|\alpha_{m,m}(0)K|^2 \\ s.t. & x_{m,n} \in \left\{ e^{j\phi}|\phi \in [0,2\pi) \right\} \end{cases}$$

(5)

where $\alpha_{m,l}(k) \in [0,1]$, $\forall k \in \{-K+1,\ldots,K-1\}$ represents an arbitrary set of weights, $r_{m,l}(.)$ is the cross-correlation between m^{th}- and l^{th}- antenna transmitting waveforms, $m,l \in \{1,2,...,M\}$. If $m = l$, $r_{m,l}(.)$ represents the auto-correlation of the mth transmitting signal. k is the different lags in cross-correlation computation. Please note that $\sum_{m=1}^{M}|\alpha_{m,m}(0)K|^2$ is the weighted energy of the waveform which is essentially the zero-lag of the auto-correlations. Since this is a constant term it can be eliminated in the objective function.

In the sequel, we propose a Weighted Block Gradient Descent (WBGD) method to solve the above optimization problem. As a first step, we split the optimization variable into several blocks. To this end, we consider the signal of each transmitter as the corresponding block, that is $\mathbf{x}_t$ ($t \in \{1,\ldots,M\}$), while other blocks are held fixed and stored in the matrix $\mathbf{X}_{-t} \triangleq [\mathbf{x}_1^T;\ldots;\mathbf{x}_{t-1}^T;\mathbf{x}_{t+1}^T;\ldots;\mathbf{x}_M^T] \in \mathbb{C}^{(M-1)\times K}$. The objective function $f(\mathbf{X})$ can then be decomposed to three terms, the first one (f_m) is independent of the optimization variable $\mathbf{x}_t$, the second (f_{au}) indicate the auto-correlation of $\mathbf{x}_t$, and the last one (f_{cr}) is its cross-correlation with the other sequences of the set $\mathbf{X}_{-t}$. Mathematically,

$$f(\mathbf{X}) = f_m(\mathbf{X}_{-t}) + f_{au}(\mathbf{x}_t) + f_{cr}(\mathbf{x}_t,\mathbf{X}_{-t}),$$

(6)

where $f_m(\mathbf{X}_{-t}) = \sum_{\substack{m,l=1 \\ m,l\neq t}}^{M}\sum_{k=-N+1}^{N-1}|\alpha_{m,l}(k)r_{m,l}(k)|^2$, $f_{au}(\mathbf{x}_t) = \sum_{k=-N+1}^{N-1}|\alpha_{t,t}(k)r_{t,t}(k)|^2$, $f_{cr}(\mathbf{x}_t,\mathbf{X}_{-t}) = 2\sum_{\substack{l=1 \\ l\neq t}}^{M}\sum_{k=-N+1}^{N-1}|\alpha_{t,l}(k)r_{t,l}(k)|^2$. Now, let $\mathbf{\Phi} \triangleq \angle\mathbf{X} \in \mathbb{R}^{M\times K}$, $\mathbf{\Phi}_{-t} \triangleq \angle\mathbf{X}_{-t} \in \mathbb{R}^{(M-1)\times K}$ and the vector $\boldsymbol{\varphi}_t \triangleq \angle\mathbf{x}_t \in \mathbb{R}^{K}$ be the phases corresponding to the matrices $\mathbf{X}$, $\mathbf{X}_{-t}$ and the vector variable $\mathbf{x}_t$, respectively. Hence, with respect to $\boldsymbol{\varphi}_t$, the optimization problem is:

$$\begin{cases} \min_{\boldsymbol{\varphi}_t} & f_m(\mathbf{\Phi}_{-t}) + f_{au}(\boldsymbol{\varphi}_t) + f_{cr}(\boldsymbol{\varphi}_t,\mathbf{\Phi}_{-t}) \\ s.t. & \phi_{t,k} \in \phi \in [0,2\pi) \end{cases}$$

(7)

To solve (7), we use GD framework, which is a first-order iterative optimization algorithm for finding a local minimum of a differentiable function. In general, the GD procedure starts with an initial solution ($\mathbf{\Phi}^{(0)}$), then at i^{th} iteration, each block ($\boldsymbol{\varphi}_t$) is updated by $\boldsymbol{\varphi}_t^{(i+1)} = \boldsymbol{\varphi}_t^{(i)} + \delta^{(i)}\Delta\boldsymbol{\varphi}_t^{(i)}$, where $\delta^{(i)}$ and $\Delta\boldsymbol{\varphi}_t^{(i)}$ are the ith iteration step size and search direction. A possible solution for step size is using *backtracking line search* [27] and the opposite direction of the gradient, i.e. $\Delta\boldsymbol{\varphi}_t^{(i)} = -\nabla f(\boldsymbol{\varphi}_t^{(i)})$ is chosen for the search direction. After updating all of the blocks, the phase matrix is updated by $\mathbf{\Phi}^{(i+1)} \triangleq [\boldsymbol{\varphi}_1^{(i+1)},\ldots,\boldsymbol{\varphi}_M^{(i+1)}]^T$. Further, the gradients of $\nabla_{\boldsymbol{\varphi}_t}f_{au}(\boldsymbol{\varphi}_t^{(i)})$ and $\nabla_{\boldsymbol{\varphi}_t}f_{cr}(\boldsymbol{\varphi}_t^{(i)})$, can be obtained using the following equations, in which $e^{-j\boldsymbol{\varphi}_l} \triangleq [e^{j\phi_{l,1}},\ldots,e^{j\phi_{l,K}}]^H \in \mathbb{C}^K$, $\widetilde{\boldsymbol{\alpha}}_{m,l} \triangleq [\alpha_{m,l}^2(-K+1),\ldots,\alpha_{m,l}^2(K-1)]^T \in \mathbb{R}^{2K-1}$ and $\bar{\mathbf{r}}_{t,l} \triangleq [r_{t,l}(K-1),\ldots,r_{t,l}(-K+1)]^T \in \mathbb{C}^{2K-1}$ sequence reverse [28]:
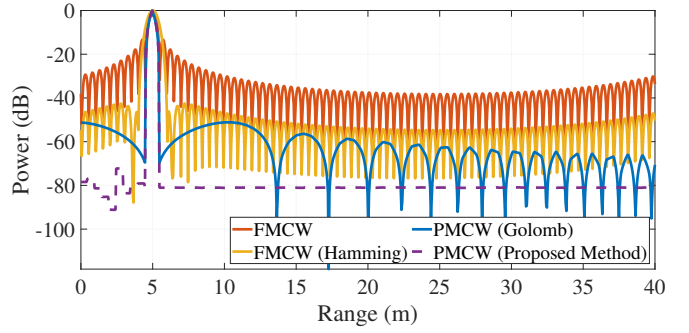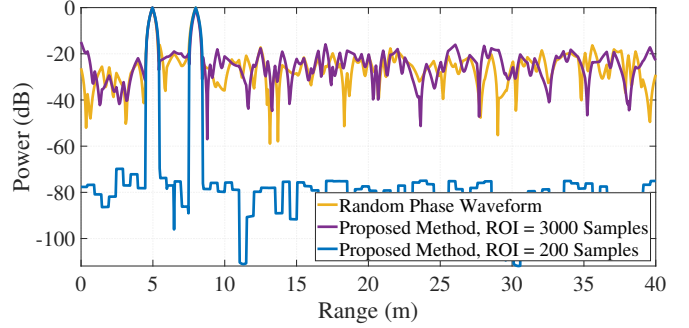

Fig. 1: Range profile for FMCW and PMCW radar

Fig. 2: Range profile for PMCW MIMO radar

TABLE II

	Range (m)	Speed (m/s)	θ (deg.)	ϕ (deg.)	σ (m²)
1	5	BPM(0.6), PMCW(7.2)	4	0	1
2	5	BPM(0.6), PMCW(7.2)	-5	0	1
3	7	BPM(0.6), PMCW(7.2)	2	0	0.2
4	5.6	BPM(0.56), PMCW(6.7)	-5	0	0.2

TABLE III

	Range (m)	Speed (m/s)	θ (deg.)	ϕ (deg.)	σ(m²)
1	5	0	0	15	1
2	5	0	12	0	1

$$\nabla_{\boldsymbol{\varphi}_t}f_{au}(\boldsymbol{\varphi}_t^{(i)}) = 4\Im[e^{-j\boldsymbol{\varphi}_t^{(i)}} \odot ((\widetilde{\boldsymbol{\alpha}}_{t,t} \odot \mathbf{r}_{t,t}) \circledast e^{j\boldsymbol{\varphi}_t^{(i)}})_{k+K-1}],$$

$$\nabla_{\boldsymbol{\varphi}_t}f_{cr}(\boldsymbol{\varphi}_t^{(i)}) = 2\Im\sum_{l=1,l\neq t}^{M}[e^{-j\boldsymbol{\varphi}_t^{(i)}} \odot ((\widetilde{\boldsymbol{\alpha}}_{t,l} \odot \bar{\mathbf{r}}_{m,l}) \circledast e^{-j\boldsymbol{\varphi}_t^{(i)}})_{k+K-1}].$$

V. SIMULATION AND RESULTS

As a case study for 4D-imaging in this section, we consider TI imaging radar (from Texas Instruments), with $L_T = 12$ Tx and $L_R = 16$ Rx channels [29], and set $B = 300$MHz, and $ROI = 100$m. In order to compare range sidelobe level and range mainlobe width of our proposed waveform with other traditional waveforms such as FMCW, Windowed FMCW (weighted by Hamming window) and Golomb sequence, we show the range profile of each waveform for Single-Input Multiple-Output (SIMO) radar in Fig. 1. The range profile for FMCW signals is the Fast Fourier Transform (FFT) of beat frequency and for PMCW signals is the matched-filter output. This figure shows that our proposed waveform has a very low sidelobe level while maintaining a narrow mainlobe
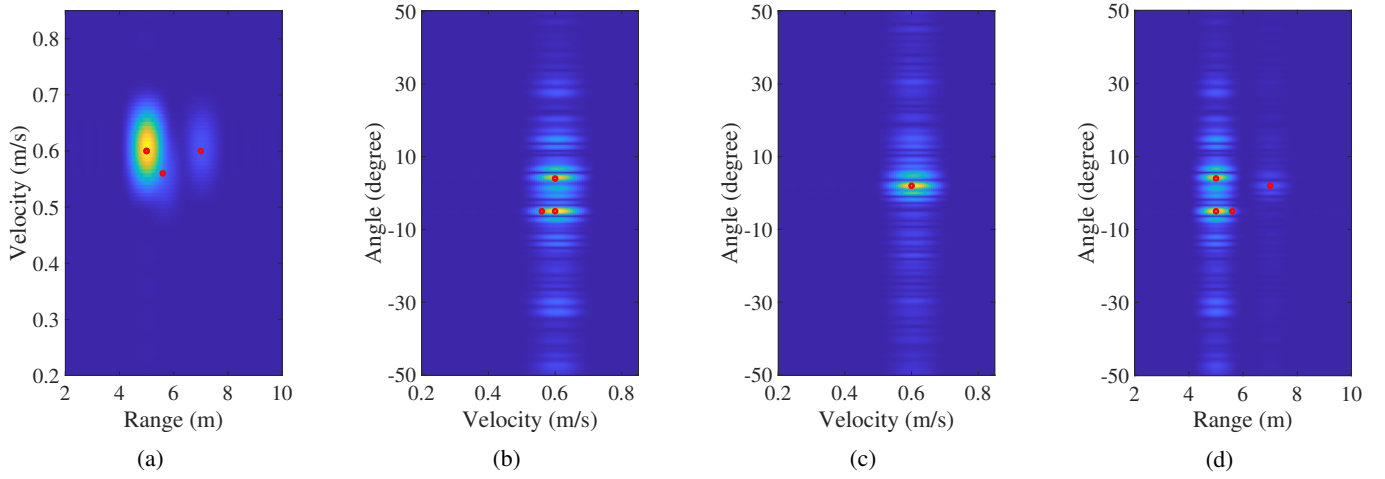
Fig. 3: BPM-MIMO (a) Range-Velocity, (b) Angle-Velocity, Range 5m, (c) Angle-Velocity, Range 7m, (d) Range-Angle.
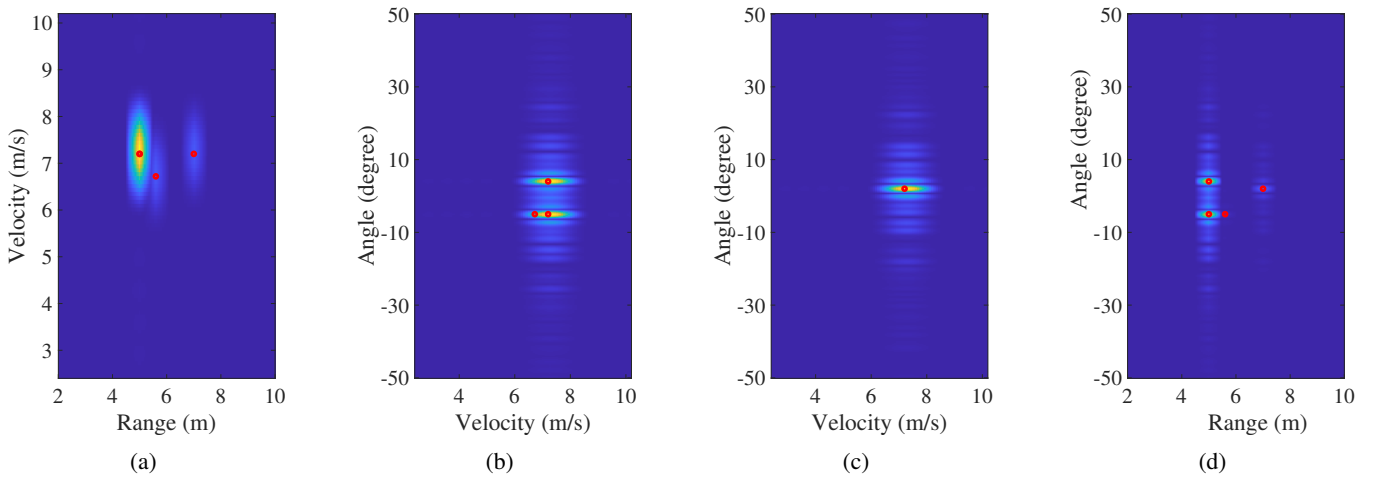

Fig. 4: Proposed Method (a) Range-Velocity, (b) Angle-Velocity, Range 5m, (c) Angle-Velocity, Range 7m, (d) Range-Angle.
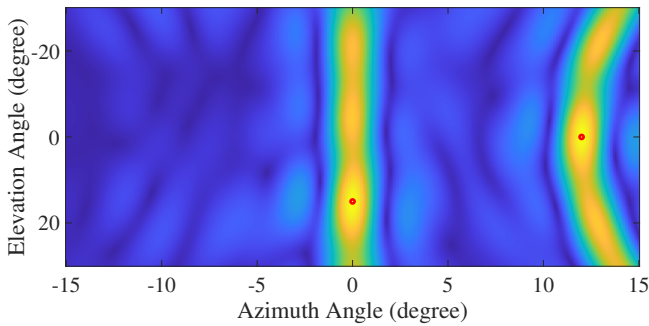

Fig. 5: Azimuth-Elevation Map

width. Despite the fact that our proposed waveform has a very high sidelobe level outside of ROI, we can perfectly use it in automotive applications due to the small required ROI. Fig. 2, illustrates PMCW waveforms (random-phase and proposed waveforms) in a 4D-imaging MIMO setting with 12 transmit antennas. The length of code sequences is set to be

3000, which is related to a pulse duration $10\mu s$. It can be seen that, by considering weights $\alpha_k = 1, k \in -K + 1, \ldots, K - 1$ (when ROI equals to the code length), our proposed method has the same performance as the random-phase sequence. On the other hand, an optimized set of sequences with a weight in the ROI (corresponding to a range of 100m), significantly reduces the range sidelobes (almost -60 dB), and outperforms the others. Finally, the performance of a PMCW MIMO radar using the sequence set optimized in this paper is compared to that of traditional FMCW radars in Fig. 3 and Fig. 4. We consider $I = 4$ targets with different parameters specified in TABLE II. The red points in these figures show the ground truth for the targets. The total number of $Q = 32$ pulses in a CPI is transmitted and also Pulse Repetition Frequency (PRF) = 10 KHz has been used for this simulation. In Fig. 3, a windowed FMCW waveform (with Hamming window) is transmitted from $M = 12$ transmit antennas with BPM-MIMO modulation. As a result of the windowing function, the mainlobe width is slightly increased. In Fig. 3a, a weak target is covered by the range sidelobes of the strong target and it is

hard to be detected. Compared to the PMCW MIMO case, the maximum unambiguous velocity is reduced with increasing the number of transmit antennas, which can be seen in Fig. 3b and Fig. 3c. These two figures, show the Angle-velocity map in two range cuts, that is $R = 5$m and 7m. Fig. 3d also shows the angle-range map, which is wide in range domain due to the windowing operation.

Compared to other existing PMCW waveforms, which have the problem of high sidelobe levels, our proposed PMCW waveform has a very low sidelobe level in the required ROI (due to the considered weights in the optimization). Thus, as it is seen in Fig. 4a, the range resolution is preserved while the weak target has been also detected in range. Due to the fast-time orthogonality based on CDM-MIMO, as another advantages of PMCW, the maximum detectable unambiguous velocity is increased. This concept is illustrated in Fig. 4b and Fig. 4c, where a Doppler velocity of M times of that in BPM-MIMO case has been detected, e.g., $0.6 \times 12 = 7.2$ m/s). Furthermore, Fig. 4d, the angle-range map, shows the better range resolution for the proposed PMCW radar. To add elevation estimation to the range-angle-velocity estimation, as in real 4D-Imaging radars, we consider two targets in the same range with the parameters defined in Table III. For the assessment of our proposed PMCW waveform, the azimuth-elevation map is depicted in Fig. 5. It can be seen that range–Doppler–azimuth–elevation estimation can be done with our proposed PMCW waveform using 2D planar array of AWR2243 4D-Imaging radar.

VI. Conclusion

In this paper, we proposed a generic signal model for different multiplexing techniques, such as TDM, DDM, CDM with Hadamard coding and fast-time CDM with PMCW waveforms. Furthermore, we introduced WBGD method to design transmit sequences with near perfect orthogonality in terms of correlation sidelobes. We simulated and compared the performance of different methods and finally, showed that the proposed WBGD technique can achieve a good performance in 4D-imaging automotive MIMO radar systems.

References

[1] R. Amar, M. Alaee-Kerahroodi, P. Babu, and B. S. M. R., "Designing interference-immune doppler-tolerant waveforms for radar systems," *IEEE Trans. Aerosp. Electron. Syst*, pp. 1–20, 2022.

[2] X. Yu, G. Cui, J. Yang, J. Li, and L. Kong, "Quadratic optimization for unimodular sequence design via an ADPM framework," *IEEE Trans. Signal Process.*, vol. 68, pp. 3619–3634, 2020.

[3] R. Amar, M. Alaee-Kerahroodi, P. Babu, and B. S. M. R, "Optimized-slope FMCW waveform for automotive radars," in *2022 23rd International Radar Symposium (IRS)*, 2022, pp. 110–115.

[4] M. Jankiraman, *FMCW Radar Design*. Artech House, 2018.

[5] F. Xu, S. A. Vorobyov, and F. Yang, "Transmit Beamspace DDMA Based Automotive MIMO Radar," *IEEE Trans. Veh. Teclnol.*, vol. 71, no. 2, pp. 1669–1684, 2022.

[6] H. Sun, F. Brigui, and M. Lesturgie, "Analysis and comparison of MIMO radar waveforms," in *2014 International Radar Conference*, 2014, pp. 1–6.

[7] Y. Sun, M. Bauduin, and A. Bourdoux, "Enhancing Unambiguous velocity in Doppler-Division Multiplexing MIMO radar," in *2021 18th European Radar Conference (EuRAD)*, 2022, pp. 493–496.

[8] A. Zwanetski and H. Rohling, "Continuous wave MIMO radar based on time division multiplexing," in *2012 13th International Radar Symposium*, 2012, pp. 119–121.

[9] J. Jung, S. Lim, S.-C. Kim, and S. Lee, "Solving Doppler-Angle Ambiguity of BPSK-MIMO FMCW Radar system," *IEEE Access*, vol. 9, pp. 120 347–120 357, 2021.

[10] A. B. Baral and M. Torlak, "Joint Doppler Frequency and Direction of Arrival Estimation for TDM MIMO Automotive Radars," *IEEE Journal of Selected Topics in Signal Processing*, vol. 15, no. 4, pp. 980–995, 2021.

[11] R. Feger, C. Pfeffer, and A. Stelzer, "A Frequency-Division MIMO FMCW Radar System Based on Delta–Sigma Modulated Transmitters," *IEEE Transactions on Microwave Theory and Techniques*, vol. 62, no. 12, pp. 3572–3581, 2014.

[12] S. Sun, A. P. Petropulu, and H. V. Poor, "MIMO Radar for Advanced Driver-Assistance Systems and Autonomous Driving: Advantages and Challenges," *IEEE Signal Processing Magazine*, vol. 37, no. 4, pp. 98–117, 2020.

[13] F. Yang, F. Xu, X. Yang, and Q. Liu, "DDMA MIMO radar system for low, slow, and small target detection," *The Journal of Engineering*, vol. 2019, no. 19, pp. 5932–5935, 2019.

[14] F. Jansen, "Automotive Radar Doppler Division MIMO With Velocity Ambiguity Resolving Capabilities," in *2019 16th European Radar Conference (EuRAD)*, 2019, pp. 245–248.

[15] M. Q. Nguyen, R. Feger, J. Bechter, M. Pichler-Scheder, M. H. Hahn, and A. Stelzer, "Fast-Chirp FDMA MIMO Radar System Using Range-Division Multiple-Access and Doppler-Division Multiple-Access," *IEEE Transactions on Microwave Theory and Techniques*, vol. 69, no. 1, pp. 1136–1148, 2021.

[16] W. van Rossum and L. Anitori, "Doppler ambiguity resolution using random slow-time code division multiple access MIMO radar with sparse signal processing," in *2018 IEEE Radar Conference (RadarConf18)*, 2018, pp. 0441–0446.

[17] O. Bialer, A. Jonas, and T. Tirer, "Code optimization for fast chirp FMCW automotive MIMO radar," *IEEE Trans. Veh. Teclnol.*, vol. 70, no. 8, pp. 7582–7593, 2021.

[18] E. Raei, M. Alaee-Kerahroodi, and M. B. Shankar, "Spatial- and range-ISLR trade-off in MIMO radar via waveform correlation optimization," *IEEE Trans. Signal Process.*, vol. 69, pp. 3283–3298, 2021.

[19] E. Raei, S. Sedighi, M. Alaee-Kerahroodi, and M. B. Shankar, "MIMO radar transmit beampattern shaping for spectrally dense environments," *IEEE Trans. Aerosp. Electron. Syst*, pp. 1–13, 2022.

[20] A. E. Ertan, K. Anderson, and M. Ali, "Cognitive radar approaches to address interference mitigation in mobility applications," in *2022 IEEE Radar Conference (RadarConf22)*, 2022, pp. 1–6.

[21] J. Overdevest, F. Jansen, F. Uysal, and A. Yarovoy, "Doppler influence on waveform orthogonality in 79 ghz mimo phase-coded automotive radar," *IEEE Trans. Veh. Teclnol.*, vol. 69, no. 1, pp. 16–25, 2020.

[22] M. Alaee-Kerahroodi, A. Aubry, A. De Maio, M. M. Naghsh, and M. Modarres-Hashemi, "A coordinate-descent framework to design low PSL/ISL sequences," *IEEE Trans. Signal Process.*, vol. 65, no. 22, pp. 5942–5956, Nov. 2017.

[23] M. Alaee-Kerahroodi, M. Modarres-Hashemi, and M. M. Naghsh, "Designing sets of binary sequences for mimo radar systems," *IEEE Trans. Signal Process.*, vol. 67, no. 13, pp. 3347–3360, July 2019.

[24] L. Wu, M. Alaee-Kerahroodi, and B. M. R. Shankar, "Improving pulse-compression weather radar via the joint design of subpulses and extended mismatch filter," in *IGARSS 2022 - 2022 IEEE International Geoscience and Remote Sensing Symposium*, 2022, pp. 469–472.

[25] E. Raei, M. Alaee-Kerahroodi, P. Babu, and M. R. B. Shankar, "Design of MIMO radar waveforms based on lp-norm criteria," 2021.

[26] H. He, J. Li, and P. Stoica, *Waveform design for active sensing systems: a computational approach*. Cambridge University Press, 2012.

[27] S. Boyd and L. Vandenberghe, *Convex optimization*. Cambridge university press, 2004.

[28] J. M. Baden, B. O'Donnell, and L. Schmieder, "Multiobjective sequence design via gradient descent methods," *IEEE Trans. Aerosp. Electron. Syst*, vol. 54, no. 3, pp. 1237–1252, 2018.

[29] "Design guide: TIDEP -01012—Imaging radar using cascaded mmWave sensor reference design (REV. A)," Texas Instruments Inc., Dallas , June 2019, [Online]. Available: http://www.ti.com/lit/ug/tiduen5a/tiduen5a.pdf.